

Ubiquitous increases in flood magnitude in the Columbia River Basin under climate change

Laura E. Queen¹, Philip W. Mote¹, David E. Rupp¹, Oriana Chegwidden², and Bart Nijssen²

¹Oregon Climate Change Research Institute, Oregon State University, Corvallis OR 97331 USA

²Department of Civil and Environmental Engineering, University of Washington Seattle WA 98105 USA

Correspondence to: Laura Queen (lqueen@uoregon.edu)

Abstract. The US and Canada have entered negotiations to modernize the Columbia River Treaty, signed in 1961. Key priorities are balancing flood risk, hydropower production, and improving aquatic ecosystem function while incorporating projected effects of climate change. In support of the US effort, Chegwidden et al. (2017) developed a large-ensemble dataset of past and future daily streamflows at 396 sites throughout the Columbia River Basin (CRB) and select other watersheds in western Washington and Oregon, using state-of-the art climate and hydrologic models. In this study, we use that dataset to present new analyses of the effects of future climate change on flooding using water year maximum daily streamflows. For each simulation, flood statistics are estimated from Generalized Extreme Value distributions fit to simulated water year maximum daily streamflows for 50-year windows of the past (1950-1999) and future (2050-2099) periods. Our results contrast with previous findings: we find that the vast majority of locations in the CRB are estimated to experience an increase in future streamflow magnitudes. We show that on the Columbia and Willamette rivers, increases in streamflow magnitudes are smallest downstream and grow larger moving upstream. For the Snake River, however, the pattern is reversed, with increases in streamflow magnitudes growing larger moving downstream to the confluence with the Salmon River tributary, and then abruptly dropping. We decompose the variation in results attributable to variability in climate and hydrologic factors across the ensemble, finding that climate contributes more variation in larger basins while hydrology contributes more in smaller basins. Equally important for practical applications like flood control rule curves, the seasonal timing of flooding shifts dramatically on some rivers (e.g., on the Snake, 20th century floods occur exclusively in late spring, but by the end of the 21st century some floods occur as early as December) and not at all on others (e.g. the Willamette).

28 **1 Introduction**

29 Among natural disasters in the Northwest, flooding ranks second behind fire in federal disaster declarations¹ since
30 1953 despite extensive flood prevention infrastructure. The largest flood in modern times on the Columbia oc-
31 curred in late spring (May-June) 1948, and obliterated the town of Vanport which lay on an island between Port-
32 land, OR and Vancouver, WA, permanently displacing its 18,500 residents². Other disruptive floods in the region
33 include the Heppner flood in 1903, one of the deadliest flash floods in US history (Byrd, 2014); floods on the
34 Chehalis River in both December 2007³ and January 2009⁴ that closed Interstate 5, the main north-south trans-
35 portation corridor through the Northwest, for several days each time at a cost of several \$m per day to freight
36 movement alone; and floods on the Willamette River in February 1996 and April 2019. The timing of typical
37 floods varies widely across the region: low-elevation basins in western Washington and Oregon typically flood
38 in November through February, whereas the snow-dominant basins east of the Cascades more typically flood in
39 spring, sometimes as late as June (Berghuis et al. 2016).

40

41 The Columbia River drains much of the Northwest, with the fourth largest annual streamflow volume in the US
42 and a drainage that includes portions of seven states plus the Canadian province of British Columbia (BC), an
43 area of 668,000 km² (Fig. 1). Its numerous federal and nonfederal dams provide flood protection, hydropower
44 production, navigation, irrigation, and recreation services. A treaty between the US and Canada, signed in 1961,
45 codified joint management of the river's reservoirs (and funded construction of new reservoirs in BC) primarily
46 to provide flood protection and hydropower production⁵. The US and Canada have entered negotiations to update
47 the treaty; the USA's "key objectives include continued, careful management of flood risk; ensuring a reliable
48 and economical power supply; and improving the ecosystem in a modernized Treaty regime." (*ibid.*) Both coun-
49 tries have expressed an intention to include the effects of climate change on streamflows, and clearly a key aspect
50 of hydrologic change is to inform the treaty negotiations of the influence of climate change on the magnitude of
51 flooding.

¹ <https://www.fema.gov/data-visualization-summary-disaster-declarations-and-grants> accessed 8/6/2019

² https://www.oregonlive.com/portland/2017/05/vanport_flood_may_30_1948_chan.html accessed 8/6/2019

³ <https://www.seattletimes.com/seattle-news/extensive-flooding-3-confirmed-deaths-hundreds-of-rescues/> ac-
cessed 8/6/2019

⁴ [https://www.seattletimes.com/seattle-news/despite-drying-cooling-trend-flooding-and-road-closures-con-
tinue/](https://www.seattletimes.com/seattle-news/despite-drying-cooling-trend-flooding-and-road-closures-con-
tinue/) accessed 8/6/2019

⁵ <https://www.state.gov/columbia-river-treaty/> accessed 8/6/2019

52

53 While rising temperatures potentially affect all parts of the hydrologic cycle, in a snowmelt-dominated hydrologic
54 system such as many of the Northwest's river basins, warming directly affects snow accumulation and melt (e.g.,
55 Hamlet et al. 2005). Observational studies have shown consistent changes toward lower spring snowpack (Mote
56 et al. 2018), earlier spring streamflow (Stewart et al. 2005), and lower summer streamflow (Fritze et al. 2011)
57 since the mid-20th century. Observations of trends in flooding in the US have generally failed to find any con-
58 sistent trends (Lins and Slack 1999; Douglass et al. 2000; Sharma et al. 2018). Sharma et al. (2018) offer several
59 possible explanations, chiefly "decreases in antecedent soil moisture, decreasing storm extent, and decreases in
60 snowmelt". The detection of trends in floods is complicated by the interaction of extreme events and nonstation-
61 arity (Serinaldi and Kilsby, 2015). Moreover, as a result of the substantial alteration of rivers to prevent flooding
62 (e.g., by the construction of dams and levees) during the observational period, the best long-term records - i.e., on
63 streams with the least modifications - are on rivers that were not producing sufficiently disruptive floods to lead
64 decision-makers to construct flood protection structures. That is, as flooding of settlements, infrastructure, or other
65 assets led to the investments in flood protection structures on most rivers, thereby altering the streamflow regime
66 and dividing any gauged records into pre- and post- modification, the ones that were left unmodified tended to be
67 small and/or remote.

68

69 To interpret the ambiguous results from observed trends, Hamlet and Lettenmaier (2007) used the Variable Infil-
70 tration Capacity (VIC) hydrologic model forced twice with detrended observed daily weather for the period 1916-
71 2003, with about 1°C of temperature difference between the two. They then compared 20- and 100-year flood
72 quantiles for basins at varying sizes in the western US and found a wide range of changes in flood magnitude
73 ranging from large decreases to large increases (+/- 30%). Broadly, the responses depended somewhat on basin
74 winter temperature, with the coldest basins (<-6°C) showing reductions in flood magnitude owing to reduced
75 snowpack, basins with moderate temperatures exhibiting a wide range of changes, and rain-dominant (>5°C)
76 basins showing little change, though the warm basins in coastal areas of Washington, Oregon, and California
77 showed increased flood magnitude.

78

79 Modeling work using state-of-the-art hydrologic models has been applied to understand where and how flood
80 magnitudes may change in the future. Tohver et al (2014) found widespread increases in flood magnitudes, espe-
81 cially in temperature-sensitive basins (mainly on the west side of the Cascades), but their approach used monthly
82 GCM output so changes in daily precipitation would not be represented. Salathé et al. (2014) used a single global

83 climate model (GCM), the ECHAM5, linked to a regional climate model to obtain high-resolution (in space and
84 time) driving data for VIC over the period 1970-2069. As did Hamlet and Lettenmaier (2007), they compared the
85 ratio of flood change (2050s vs 1980s) against mean historical winter temperature and found a majority of loca-
86 tions with a higher 100-year flood, in some cases by a factor of 2 or more; while they projected increases in every
87 one of the warmer basins ($>0^{\circ}\text{C}$), a substantial fraction of colder locations had decreases in flood magnitude.

88
89 Chegwiddden et al. (2019) describe the process used to generate the streamflow ensemble used here. In addition,
90 they used analysis of variance (ANOVA) to analyze the different influences of choices of emissions scenario (as
91 a Representative Concentration Pathway - RCP), GCM, internal (unforced) climate variability, downscaling
92 method, and hydrologic model, and how those influences varied spatially across the domain and also seasonally
93 and by hydrologic variable. They found that the RCP and GCM had the largest influence on the range of annual
94 streamflow volume and timing, and hydrologic model had the largest influence on low streamflows. The hydro-
95 logic variables they considered were snowpack (maximum snow water equivalent and date of maximum SWE),
96 annual streamflow volume, centroid timing (the date at which half the water year's streamflow has passed), and
97 seasonal streamflow volume; primary focus was on centroid timing, annual volume, and minimum 7-day stream-
98 flow. They did not examine high-flow extremes that can lead to flooding. The purpose of this paper is to address
99 this important gap in our understanding of the future Northwest hydrology; to do so, we use the largest available
100 ensemble of climate-hydrology scenarios. By using a large ensemble, we ensure a reasonable breadth of climatic
101 and hydrological futures in order to better describe the range of possible future flooding and how it varies across
102 the region with its diverse hydroclimates.

103 **2 Methods**

104 **2.1 Hydrologic modeling data set**

105 To assess changing flood magnitudes under climate change, we analyzed changes in water year maximum daily
106 streamflows in a large ensemble of streamflow simulations at 396 locations in the CRB (Figure 1) and select
107 watersheds in western Oregon and Washington (Chegwiddden et al., 2017). The simulations were constructed from
108 permutations of modeling decisions on forcing datasets and hydrologic modeling. Specifically, choices included
109 two RCPs (RCP4.5 and RCP8.5), ten GCMs, two methods of downscaling the climate model output to the reso-
110 lution of the hydrologic models, and four hydrologic model implementations, for a total of 160 permutations. For
111 our analysis, we extracted a more tractable dataset of 40 simulations per location, by only considering simulations

112 with RCP 8.5 and the Multivariate Adaptive Constructed Analogs (MACA) downscaling method (Abatzoglou
113 and Brown, 2012).

114

115 The rationale for using a subset of the available data is as follows. First, the time-dependent set of greenhouse gas
116 concentrations in RCP4.5 is fully included in RCP8.5, so any concentration of greenhouse gases on the RCP4.5
117 path can be converted to a point on RCP8.5 (at a different time). We analyzed results for both RCP8.5 and RCP4.5,
118 and found that to first order the changes in flood magnitude in RCP4.5 were approximately 2/3 those in RCP8.5,
119 which is also roughly the ratio of global temperature change over the period considered (IPCC Summary for
120 Policymakers, 2014). For clarity we show only the results for RCP8.5. Second, we considered only simulations
121 using the MACA downscaling method because of the method's ability to capture the daily GCM-simulated me-
122 teorology critical for assessing changes in extremes and its skill in topographically complex regions (Lute et al.,
123 2015). The other downscaling approach used by Chegwiddden et al. (2019), the Bias Correction and Statistical
124 Downscaling (BCSD) method (Wood et al. 2004), produces probability distributions of daily precipitation incon-
125 sistent with the GCM response to forcings because the method stochastically disaggregates monthly data to daily
126 data based on historical statistical properties of the daily data. This statistical property limits the ability of BCSD
127 to reproduce changes in storm frequency in the future, making it a less attractive choice for daily extreme stream-
128 flow analysis (Hamlet et al. 2010; Guttman et al. 2014).

129

130 Model output used in this study came from the following ten GCMs: CanESM2, CCSM4, CNRM-CM5, CSIRO-
131 Mk3-6-0, GFDL-ESM2M, HadGEM2-CC, HadGEM2-ES, Inmcm4, IPSL-CM5A-MR, and MIROC5. These ten
132 GCMs were chosen primarily for their ability to accurately reproduce observed climate metrics during the histor-
133 ical period mainly of the Northwest US but also at sub-continental and larger scales as assessed in Rupp et al.
134 (2013) and RMJOC (2018). The four hydrologic model implementations originated from two distinct hydrologic
135 models: the Variable Infiltration Capacity (VIC; Liang et al., 1994) model and the Precipitation Runoff Modeling
136 System (PRMS; Leavesley et al., 1983). VIC and PRMS are process-based, energy balance models and were both
137 run on the same 1/16th degree grid with output saved at a daily time step for the period 1950 to 2099. VIC is a
138 macroscale semi-distributed hydrologic model that solves full water and energy balances, and in these simulations
139 it also included a glacier model (Hamman & Nijssen, 2015). Three unique implementations of VIC were used
140 with independently derived parameter sets (P1, P2, P3) marked by differences in calibrated parameters, calibration
141 methodology, and meteorological and streamflow reference sets. PRMS is a distributed, deterministic hydrologic

142 model which, in contrast to VIC, does not allow for subgrid heterogeneity. See Chegwidden et al (2019) for
143 details. It is important to note that these hydrologic simulations and calibrations do not include reservoir models.

144 **2.2 Flood magnitude**

145 We assessed changes in flood magnitude in the Columbia River Basin by comparing water year maximum daily
146 streamflows over a 150-year period (1950-2100). We estimated the 10, 5, 2, and 1% probability of occurrence
147 (commonly referred to as the 10-, 20-, 50-, and 100-year flood, respectively) by fitting generalized extreme value
148 (GEV) probability distributions to simulated water year maximum daily streamflows for 50-year windows of the
149 past (1950-1999) and future (2050-2099) periods; see Figure 2 for an example. (We also looked at 30- and 75-
150 year windows, choosing 50 years as a balance between sample size favoring longer periods, and nonstationarity
151 considerations favoring shorter periods.) We used Python’s `scipy.stats.genextreme` module (Jones et al., 2001) to
152 fit a Gumbel distribution and estimate flood magnitudes for each return period. We assessed change in flood
153 magnitude as the “discharge ratio” of the estimated future to past floods for a given return period; a ratio greater
154 than 1 indicates an increase in flood magnitudes while a ratio less than 1 indicates a decrease.

155
156 We describe how changes in flood magnitude vary by climatic zone across the PNW by using an efficient and
157 internally consistent proxy for climatic zone: the centroid of timing – the day in the water year that half the annual
158 volume of water has passed the stream location. The centroid of timing is a metric of snow dominance (e.g.,
159 Stewart et al. 2005) which is related to the spatial distribution of temperature and tends to decrease downstream.
160 This temporal proxy of a hydrologic characteristic is effective in the Columbia Basin where most of the precipi-
161 tation occurs in winter and the relative magnitude and timing of the freshet from the spring thaw is a good indicator
162 of importance of snowmelt to streamflow. An early centroid indicates that rain, which falls predominantly during
163 the cooler, earlier part of the year, is the driver of the peak streamflows at the location, while a late centroid
164 indicates that snowmelt during later spring months is the prime hydrological driver. We computed the centroid
165 using the 1950-79 simulated years. Note that Chegwidden et al. (2019) also used the *change* in centroid as a
166 hydrologic variable of interest; below, we discuss our results in the context of their findings.

167

168 **2.3 Model evaluation**

169 Comparing directly between gauged flows and modeled flows is inadvisable since the observed streamflows are
170 substantially altered by regulation, which is not accounted for in the hydrological model. However, a set of stream-

171 flows called No Reservoirs No Irrigation (NRNI; RMJOC 2017) has been developed by federal agencies to sup-
172 port practical analysis. The NRNI dataset exists at ~190 sites across the Columbia River Basin for the years 1928-
173 2008, and streamflows are adjusted to correct for reservoir management and the diversions and evaporation asso-
174 ciated with both the reservoirs and with irrigated agriculture. This dataset is suitable for comparisons with our
175 modeling setup, and we have computed return period curves using GEV fits at all the NRNI locations (not shown)
176 for the period common to both NRNI and our ensemble, viz., 1950-2008. From these fits we have estimated the
177 10-year and 100-year values (Figure 3). On the lower mainstem Columbia (Figs 3a and d), the return period curves
178 are very close to those computed from NRNI and the means of simulations are almost all within 8% of the NRNI
179 values. Individual hydrologic model configurations are not consistently biased across the basin nor across return
180 periods; despite its different provenance, PRMS generally lies within the return period streamflows of the three
181 VIC configurations rather than being consistently different from all VIC configurations, although the lowest val-
182 ues are from PRMS. On the Snake River, the mean of modeled high streamflows range from 5% above NRNI at
183 Little Goose to 24% above at Oxbow for 10-year floods (and 14% to 41% for 100-year) but again no hydrologic
184 model stands out as strongly biased. On the Willamette, however, the modeled 10-year and 100-year flood mag-
185 nitudes lie almost entirely below NRNI and the means are too low by from 30% (T. W. Sullivan, 10-year) to 50%
186 (Hills Creek, 100-year). PRMS and the P2 calibration of VIC are consistently closer to NRNI on the Willamette.
187 It is worth stressing that these results compare outputs of hydrologic models in which the inputs are simulated
188 daily weather (which is then bias-corrected) rather than observed daily weather, and that the hydrologic models
189 are calibrated to 7-day means rather than the daily values relevant here. In general, the simulated flood statistics
190 are least biased on larger river reaches where the hydrographs are less flashy. For the Columbia mainstem, there
191 is good agreement with extreme high streamflows in the NRNI dataset.

192
193 We also examined the ensemble performance for 1950-2008 in the distribution of timing of peak daily streamflow
194 for 28 locations along the Columbia, Snake, and Willamette (a subset is shown in Figure 4). At all locations we
195 examined, the median date (as well as earliest and latest quartiles) of annual maximum daily streamflow in the
196 ensemble is within 10 days of the observed, from NRNI. The modeled distribution is shifted slightly later than
197 NRNI on the lower Columbia and slightly earlier than NRNI on the Willamette. As with magnitudes, the agree-
198 ment in timing suggests a robust modeling set-up since the comparison tests the ability of the combined climate-
199 hydrologic modeling system to match observed, constrained only by the broad physics of the climate system and

200 by meteorological bias correction (which cannot substantially change the timing of the day of the year most con-
201 ducive to high streamflows). Although the modeled streamflows are calibrated, the statistical approach to calibra-
202 tions is not sensitive to the extreme maximum daily streamflow studied here.

203 **3 Results**

204 **3.1 Regional changes in flood ratio**

205 Figure 5 shows the changes in maximum daily discharge for all of the 396 streamflow locations for different
206 return periods. The horizontal position of each circle represents the centroid of timing. The circles are semi-opaque
207 so overlapping circles lead to a deeper saturation. Points on the same river are ordered from more to less snow
208 dominant (i.e., right to left) traveling downstream; strings of circles in a smooth pattern usually indicate one of
209 the larger rivers, highlighted in Figure 6. Each circle in Figures 5 and 6 represents an average of 40 simulations:
210 10 GCMs and 4 hydrologic model configurations.

211
212 A striking result in Figure 5 is that, in contrast to the results of Tohver et al. (2014), the flood magnitude increases
213 (i.e., the discharge ratio exceeds one) at nearly every streamflow location and return period (though not for every
214 individual climate scenario, as shown in Figure 7). Broadly, the patterns are similar across all return periods
215 though with slightly higher ratios for longer return periods, and subsequent figures will show only the 10- and
216 100-year floods. For the streamflow locations with centroid <125 or so (i.e. February 2), flood ratios are fairly
217 concentrated about 1.25 for all return periods. For mixed rain-snow basins, roughly delineated by centroids be-
218 tween 125 and 160 (March 8 most years), flood ratios range widely from just below 1 to about 2.4 for the 10-year
219 and 3.2 for 50- and 100-year floods. For the longer return intervals, there is a wide range of projected changes in
220 daily flood at many locations (indicated by the red coloring). This is undoubtedly partly due to the GEV fit ex-
221 trapolating from 50 to 100 years. Finally, for the basins with streamflow centroid >160 , the ratios have a smaller
222 range, from slightly greater than 1 to a maximum that increases from about 2 for the 10-year, to about 2.75 for
223 100-year. Tohver et al. (2014) distinguished basins by their DJF temperature, a rough proxy for our snow domi-
224 nance metric, and found a substantial number of locations where the flood ratio for both 20-year and 100-year
225 flood was as much as 20% lower for the 2040s compared with a historical period. We return to this point in the
226 conclusions.

227

228 To understand better how flood magnitude changes along the length of a river, we focus (Figure 6) on a handful
229 of significant rivers in the region: the mainstem Columbia, Willamette (along with major tributaries the McKenzie
230 and Middle Fork Willamette), and Snake, and also on the Chehalis in southwest Washington (see Introduction).
231 Flow locations and select numerical results are listed in Table 1. Many of the larger tributaries also have stream-
232 flow points in our dataset, so we can infer the role of tributaries in changing the flood magnitudes in the future,
233 as discussed below. The Columbia River includes the most snow-dominant basins, with a centroid of >190 days
234 (early to mid April) in the Canadian portion of the basin. The flood ratio decreases almost uniformly along the
235 length of the river, from 1.3 for the 10-year and >1.5 for the 100-year in the Canadian portion to just above 1 at
236 the last few points along the river (The Dalles, Bonneville, and Portland). Past flood events on the mainstem
237 Columbia are exclusively associated with large spring snowmelt, and the large tributaries (the Yakima, Snake,
238 and Willamette) contribute annual streamflow volume but rarely contribute peak streamflow at the same time; as
239 shown below, the future flood timing changes but flood magnitudes change little in the lower Columbia owing to
240 the fact that the Columbia integrates such diverse hydroclimates. Like the Columbia, the Willamette also has
241 flood ratios that decrease along the length of the river as it integrates more diverse hydroclimates, from 1.7 to 1.35
242 for both return periods. The McKenzie River (points 15-17), one of the three tributaries that converge at Eugene
243 to form the Willamette, is a highly spring-fed river with higher baseflow than is represented in the hydrologic
244 models, though it is unclear how that difference would manifest in the flood statistics.

245

246 In contrast to the Columbia and the Willamette, the Snake behaves oppositely: flood ratio increases downstream
247 along the length of the river, until the confluence with the Salmon River, which drains a large mountainous area
248 of central Idaho. On parts of the Snake the ratios are as high as 1.4 for 10-year and 1.6 for 100-year. Then after
249 the confluence with the Salmon River, which has much lower change in discharge ratio, the ratios on the Snake
250 drop to about 1.2 for 10-year and about 1.3 for the 100-year. Our hypothesis is that in the Snake above the Salmon
251 River, the tributaries shift from snow-dominant to rain-dominant, so that a single storm can drive large rainfall-
252 driven increases (possibly with a snowmelt component) leading to larger synchronous discharges. The Salmon
253 and Clearwater rivers retain less exposure to such shifts, and dilute the effects of single large storms on flooding.

254

255 Each circle in Figures 5 and 6 represents an average of 40 simulations: 10 GCMs and 4 hydrologic model config-
256 urations. To better understand the range in results, Figure 7 shows the discharge ratio for all 40 simulations at
257 each point on the mainstem Columbia. Although the mean flood ratio at the lowest two points is only barely above

258 1, several ensemble members have ratios less than one, and a few have ratios >1.5 . Moving upstream, the range
259 in results increases, as shown also by the color of the dots.

260 **3.2 Dependence of results on modeling choices**

261 As in Chegwiddden et al (2019), we separate the results - here for the three largest rivers - into variations across
262 GCM (Figure 8) and variations across hydrologic model configurations (Figure 9). The ranking of flood ratios by
263 GCM changes substantially between basins and even within a basin, and does not correspond to the changes in
264 seasonal precipitation. For the upper Columbia River, the models with the least warming - inmcm4 and GFDL-
265 ESM2M (Rupp et al 2017) - have almost no change in flood magnitude, but the HadGEM2-ES which warms
266 considerably in summer produces a large decrease in flood magnitude. In the Willamette and Snake Rivers, the
267 range of projected flood changes by different GCMs remains large from the headwaters to the mouth of the river,
268 whereas for the Columbia the range diminishes considerably as one moves downriver.

269
270 The variation of results depends less on hydrologic model than on GCM (Figure 9), though the differences across
271 hydrological models are still substantial. For the Willamette, lower Snake, and both upper and lower Columbia,
272 the PRMS model predicts substantially larger increases in flooding than the three calibrations of the VIC model.
273 For the upper Snake, it predicts substantially smaller change than any VIC calibration. While it is perhaps not
274 surprising that the three calibrations of VIC are close to each other, it is striking just how different are the projec-
275 tions from PRMS at most locations on these three rivers. Chegwiddden et al. (2019) found that the main contribu-
276 tors to differences in hydrologic variables (except low streamflows) generally were the climate scenarios (GCM
277 and RCP), consistent with our findings here. (The order of models is similar in the equivalent figure for the 100-
278 year return period, but we elected to show the 10-year figure since the 100-year figure is more difficult to decipher
279 because the symbols overlap with those from other rivers.)

280
281 To parse the contributions of climate factors (represented by the GCMs) and hydrologic factors (represented by
282 the hydrologic models), we perform ANOVA on the 40 discharge ratios. The pie charts in Figure 10 show the
283 proportion of the total variance explained by climate factors and hydrologic factors at different locations. For the
284 Willamette River, the portion of uncertainty connected to the climate grows more important and the portion of
285 uncertainty connected to the hydrologic variability less important going from the confluence of the three major
286 tributaries at Eugene to the mouth. For the Snake and Columbia rivers, climate is responsible for virtually all of
287 the variance in projections in the upper reaches, but only about half at the lowest point, similar to the Willamette.

288 The Willamette basin is much smaller, and a large storm can affect the entire basin on the same day (Parker and
289 Abatzoglou, 2016), whereas storms typically take a couple of days to move across the Snake and Columbia (and
290 generally move upstream). With larger and more diverse contributing areas, differences in the rates with which
291 the hydrological models transfer precipitation to the point of interest become more important. Unlike Chegwid-
292 den et al. (2019), we did not attempt to isolate the response to anthropogenic forcing from internal climate variabil-
293 ity. Though several techniques for separating these two factors have been used (e.g., Hawkins and Sutton, 2009;
294 Rupp et al., 2017; Chegwid- den et al., 2019), these techniques are either infeasible with our dataset or we question
295 their suitability for the application to changes in extreme river flows.

296 **3.3 Change in timing**

297 Although in a broad hydrologic sense a flood is a flood regardless of what time of year it occurs, there are poten-
298 tially significant ecological differences depending on time of year; for example, scouring the river bottom causing
299 significant loss of salmon eggs (Goode et al. 2013). Moreover, water management policies are strongly linked to
300 the calendar year (see Discussion). We computed the probability of flooding for (all 40) past and future simula-
301 tions at all the points on the three rivers (Figure 6) as a function of day of year (Figure 11). For the Willamette,
302 no significant change in timing occurs; however, for the upper Willamette, a single peak in likelihood in February
303 becomes more diffuse. For the Snake, all locations see a shift toward earlier floods, consistent with the transition
304 to less snow-dominant and more rain-dominant. Whereas floods were historically concentrated in the period of
305 mid-May to mid-July, the projected future flooding period spans December to June. For the Columbia, the mode
306 in the flood timing shifts earlier by half a month in the upper Columbia to about a month in the lower Columbia.
307 The distribution also broadens with an elongated tail towards winter such that there is low, but non-negligible,
308 probability of floods occurring as early as January. The magnitudes of the 10- and 100-year flood events in the
309 lower Columbia are not projected to increase substantially (Figures 6-9). However, the window during which a
310 major flood could occur expands, with the likelihood of major flooding in May or April (or even as early as
311 February) increasing.

312 **4 Discussion and conclusions**

313 Our study joins a small number of others in examining high-flow extremes using a large hydroclimate ensemble.
314 Gangrade et al. (2020) used a similar ensemble approach analyzing hydrological projections for the Alabama-

315 Coosa-Tallapoosa River Basin with 11 dynamically downscaled and bias corrected GCMs (10 of which our stud-
316 ies share) and 3 hydrologic models (including VIC and PRMS). While they did not examine extreme daily stream-
317 flows, they did calculate changes in the 95th percentile of daily streamflow (Q95). Perhaps because of the hydro-
318 climatic uniformity of that basin, they found very small differences in Q95 across hydrologic models, which
319 contrasts with our results showing changes in flood magnitudes varying by watershed and distance downstream.
320 Thober et al. (2018) conducted a similar study in some European river basins, but rather than using a climate
321 ensemble they simply imposed uniform warming scenarios on a hydrologic model (i.e. a more straightforward
322 temperature sensitivity analysis rather than an exploration of the range of future climate scenarios). Other, smaller
323 ensemble studies of floods in different basins include Huang et al. (2018), with 4 GCMs and 3 hydrology models,
324 and Vormoor et al (2015) with several parameterizations of one hydrology model.

325
326 Returning to the Northwest, our findings contrast with earlier work. Salathe et al. (2014) found decreases in flood
327 magnitude at a substantial number of sites, but our results show increases in flood magnitude at nearly every
328 return period and location, which includes about 100 locations not included in their study. They also noted that
329 directly downscaling the GCM outputs leads to a smaller range of results than when running the regional model
330 as an intermediate step, so we infer that if we had had access to RCM simulations driven by all 20 of our RCP-
331 GCM combinations, our range of results might have been larger. Another important difference may be in the
332 spatiotemporal coherence of extreme precipitation, which in the RCM would be generated directly by the inter-
333 action of synoptic-scale storms, topography, and to a small extent by surface water and energy balance; and in
334 our study, by the interaction of the GCM-scale synoptic storms and constructed analogs derived from observa-
335 tions. A large ensemble would reduce the magnitude of that effect. In our study, the MACA statistical downscaling
336 approach preserves much of the daily variability from the GCM, so the primary reason for the difference between
337 our results and theirs is probably the fact that we analyzed 40 scenarios. Some locations, for example the points
338 on the lower Columbia river, had a handful of ensemble members with decreasing flood magnitude. But averaging
339 the entire ensemble nearly always resulted in an increase in flood magnitude. It is possible therefore that their
340 study, repeated with a larger ensemble of hydrologic-climate model combinations, might have found ubiquitous
341 increases in flood magnitude as ours did.

342
343 Prior results (Hamlet and Lettenmaier 2007, Tohver et al. 2014, Salathe et al. 2014) suggested a decrease in flood
344 magnitude in snowmelt-dominated basins like the Columbia, since reduced snowpack reduces the store of water
345 available to be released quickly in a spring flood (like the May-June 1948 Vanport flood). In a subbasin of the

346 Willamette, Surfleet and Tullos (2013) projected decreases in flood magnitude for return periods > 10 years in the
347 Santiam River basin under a high-emissions scenario (SRES A1B, 2070-2099 vs. 1960-2010; 8 GCMs), attrib-
348 uting the decreases to fewer large rain-on-snow events. Our results for the Santiam River show an *increase* of
349 40% for both 10- and 100-year floods; this result includes rain-on-snow events, since they are represented in VIC,
350 which computes the accumulation of water in the snowpack and determines whether sufficient energy has been
351 provided to create a melt event. Our results point to ubiquitous increases in magnitude throughout the basin, even
352 on the lower mainstem Columbia. We also project some large increases in flood magnitude in the coldest basins,
353 including the headwaters of the Columbia, suggesting that the former results were missing some key details. It
354 seems likely that any reduction in flood magnitude originating from the warming-induced reduction in spring
355 snowpack is offset by other factors. While there is evidence that warmer future temperatures could engender
356 slower melt rates (Musselman et al. 2017), the effect on high streamflow events is less clear. For example, Cheg-
357 widden et al (2020) showed that magnitudes of both rain- and snowmelt-driven floods are likely to increase across
358 headwater basins in the Pacific Northwest through the 21st century. These results emphasize the necessity of
359 revisiting reservoir rule curves, which are strongly tied to historical hydrographs, and also emphasize that changes
360 in the seasonality of flooding can be dramatically different from the changes in the mean hydrograph. In particular,
361 in the lower Snake and lower Columbia, changes in magnitude of flooding are modest but changes in timing of
362 the earliest quartile of flood events is much larger than the 0.5-1 month shift in the mean hydrograph.

363
364 A strength of our study compared with earlier studies is the use of a large ensemble, which samples a wide climate
365 space by using GCMs as opposed to RCMs. Conventional wisdom and evidence from the weather and seasonal
366 climate forecasting realms illustrate the utility of considering ensembles, and that generally the true outcome of a
367 prediction lies near the middle of the ensemble. Our ANOVA analysis (Figure 10) shows that climate scenarios
368 contribute a majority of the variation among results for most of the basin. Consequently, it is of great importance
369 to sample the climate scenarios broadly, which currently only GCMs can do. Large ensembles of RCMs are rare;
370 the 12-member NARCCAP ensemble (6 RCMs, 4 GCMs; Mearns et al. 2013), some of whose model runs were
371 completed a decade ago, remains the largest, but has a spatial resolution of only 50km. CORDEX North America,
372 similarly now has a comparable-size ensemble, but mostly still at 50 km (some at 0.22°), and was not available in
373 such large numbers when we began our hydrologic simulations. At such spatial resolutions, RCMs would still
374 have to be further downscaled and bias corrected to use in our hydrologic models (~6km spatial resolution). In
375 the tradeoff between breadth of climate scenarios and spatial resolution, these ensembles offer insufficient im-
376 provement in spatial resolution relative to our GCM ensemble to justify sacrificing the breadth in climate scenarios

377 represented by choosing just 4 GCMs. While RCMs certainly have their place in such work and were used in
378 some previous studies, using GCMs in this study allowed for a larger climate space to be sampled, thus adding to
379 the robustness of our results.

380

381 Although the likeliest outcome, as shown in Figure 7, is for smaller changes in flood magnitude in the lower
382 Columbia, a prudent risk management strategy would consider the range of possibilities. The validation (Figures
383 3 and 4) provides no *a priori* basis for excluding or under-weighting the projections from any hydrologic model.
384 On the Willamette, a rain-dominant basin, our hydrologic simulations of flood magnitudes are biased substantially
385 ~~biased undershoots the observed flood magnitudes. It is beyond the scope of this paper to investigate the reasons,~~
386 ~~but possible causes include a low bias in extreme daily precipitation, soil parameters relevant to rare flashy events,~~
387 ~~undersimulation of rain on snow melt, or the absence of a groundwater component in the hydrologic models~~
388 ~~(while the Willamette flow in late summer has a substantial contribution from the high Cascades aquifer). Whether~~
389 ~~this low bias affects the results for the responsiveness to future change in magnitude depends in part on the im-~~
390 ~~portance of these and other factors.~~ Possible causes for the low bias originate both in the climate and hydrological
391 models. For example, a low bias in extreme daily precipitation may lead to an underestimation of the hydrologic
392 response. We also note that the hydrologic models were calibrated to 7-day means rather than daily values and
393 may underestimate the daily response in smaller basins. Nevertheless, three physical processes contribute directly
394 to the increase in magnitude: an increase in seasonal precipitation affecting soil saturation, an increase in extreme
395 daily precipitation, and a warming-induced reduction in the snow-covered area in the wet season. In our results
396 for the Willamette this reduction in snow-covered area reduces the buffering effect of snow accumulation during
397 storms and more than offsets an increase in melt from rain-on-snow events. This mechanism is supported by
398 Chegwiddden et al (2020) who, using the same underlying dataset as our study, project a growth in both prevalence
399 and magnitude of rain-driven floods at the expense of floods from snowmelt and rain-on-snow events.

400

401 Our findings provide an initial indication of how existing flood risk management could respond to a warming
402 climate. Reservoir management is guided by rule curves which are intended to reflect the changing priorities and
403 risks during the year. For example, reservoirs used for flood control have rule curves that require reservoir levels
404 to be lowered when approaching the time of year when flood likelihood increases, and reservoir levels may be
405 raised as the likelihood decreases. For the Willamette, we found little change in the distribution of timing of flood
406 events, which indicate that with the state of the science today, reservoir rule curves may need to be altered as to
407 magnitude of flooding (which our results indicate will increase by 30-40%) but not timing; a reservoir model,

408 along with further investigation of the low bias in observed flood magnitudes (Figure 3e and 3f) would be required
409 for complete understanding of how flood risk (magnitude and timing) will actually change. For the Snake, larger
410 shifts in the timing imply a need to completely re-evaluate the existing rule curves. For the Columbia, the mode
411 in flood timing shifts earlier by half a month in the upper Columbia to about a month in the lower Columbia. The
412 distribution also broadens, with an elongated tail towards winter such that there is low, but non-negligible, prob-
413 ability of floods occurring as early as January. These changes in timing imply a need for moderate alteration of
414 rule curves for reservoirs in the Canadian portion of the Columbia Basin.

415
416 Our results should not be taken as a precise prediction of flood magnitude change but rather as the best available
417 projections given the current state of the science. Two important factors need to be considered when interpreting
418 our results: first, in using RCP8.5, we selected the most extreme emissions scenario. If efforts to stabilize the
419 climate before 2050 are successful, the flood magnitudes shown here will undoubtedly be smaller (our analysis
420 suggests most of the locations would see a change in flood magnitude about 1/3 smaller, for RCP4.5; e.g., a ratio
421 of 1.3 (30% increase) for RCP8.5 would correspond to a ratio of 1.2 for RCP4.5).

422
423 The second important factor in interpreting our results is that the actual river system in the Northwest includes
424 many dams, a majority of which have flood control as a primary (or at least a top) objective. As a result, actual
425 streamflows (and the changes in streamflow) at a given point in the river would be altered by reservoir manage-
426 ment. Translating these changes in flood magnitude into actual changes would require a reservoir model for the
427 basin or subbasin of relevance. One could then compute optimal rule curves for the major flood control reservoirs
428 (perhaps time-evolving every couple of decades, to reflect the likely changes in scientific understanding and emis-
429 sions trajectory). Even without that additional analysis, however, our results stress that the magnitude and/or
430 timing of flood events will change throughout the basin. In other words, what worked for flood control in the past
431 will not work as well in the future.

432
433 This study may have some utility in framing and quantifying the possible changes in flood risk as the Columbia
434 River Treaty is in renegotiation, but further work would be needed to assign probabilities to future flood magni-
435 tude. Such work includes (a) a deeper understanding of the underlying model differences to explain differences
436 in model sensitivities (our analysis in section 2.3 shows that PRMS performs about as well as the three calibrations
437 of VIC for simulating past peak streamflows, but more work would be needed to understand the reasons for
438 divergence in future projections), (b) applying different statistical and/or dynamical downscaling methods, and

439 (c) using a more sophisticated approach to evaluating extremes in a nonstationary climate (as advocated by
440 Serinaldi and Kilsby, 2015). The mechanisms of flooding in the upper Columbia and elsewhere are also a key
441 question arising from this work; this and other work is needed to decipher the cause of the discharge ratio patterns
442 we found along the major rivers. Furthermore, a new generation of GCM outputs (CMIP6, Eyring et al. 2016)
443 already has data available from over 25 GCMs; in the near future, it would be feasible to apply a newer multi-
444 model hydrologic modeling approaches (e.g., Clark et al., 2015) to the new generation of GCMs, though perhaps
445 no significant changes would result.

446

447 Nonetheless, with current knowledge the fact that very few locations would see a decrease in flood risk under any
448 climate/hydrologic scenario is a strong statement of the need to update all aspects of flood preparation: the defi-
449 nition of N-year (especially 100-year) return period streamflows, flood plain mapping, and reservoir rule curves,
450 to name a few. Moreover, the challenges that the renegotiated Columbia River Treaty faces in accounting for
451 climate change now appear to include the necessity of incorporating the likely increase in flood risk throughout
452 the region.

453

454 Generally, this study shows how complex the spatial and temporal patterns of change can be in a mixed rain-and-
455 snow basin. Basins of similar size and hydrological response to warming exist on most continents, so our results
456 provide a warning against using a small number of climate scenarios or a single hydrologic model to estimate
457 changes in flood risk in other basins.

458

459

460 **Code/data availability.** The data used here are available at <https://zenodo.org/record/854763>.

461

462 **Author contribution.** L. Queen performed all analyses, wrote portions of the text, and edited the document. P.
463 Mote guided the analysis and wrote much of the text. D. Rupp guided the analysis and edited the document. O.
464 Chegwiddden generated the underlying dataset, guided the analysis, provided assistance with programming, and
465 commented on the text. B. Nijssen generated the underlying dataset and commented on the text.

466

467 **Competing interests.** The authors declare no competing interests.

468

469 **Acknowledgments.** This project originated as a senior honors thesis by the first author, who
470 thanks Hank Childs of the University of Oregon for his mentorship. The research was sup-
471 ported by the NOAA Climate Impacts Research Consortium, under award
472 #NA15OAR4310145. We acknowledge the World Climate Research Programme’s Working
473 Group on Coupled Modelling, which is responsible for CMIP, and we thank each respective
474 climate modeling group for producing and making available their model output. For CMIP
475 the U.S. Department of Energy's Program for Climate Model Diagnosis and Intercomparison
476 provides coordinating support and led development of software infrastructure in partnership
477 with the Global Organization for Earth System Science Portals.
478
479

480 **References**

481

482 Addor, N., Rössler, O., Köplin, N., Huss, M., Weingartner, R., & Seibert, J. (2014). Robust changes and sources
483 of uncertainty in the projected hydrological regimes of Swiss catchments. *Water Resources Research*, 50(10),
484 7541-7562.

485

486 Berghuijs, W.R., R.A. Woods, C.J. Hutton, and M. Sivapalan, Dominant Flood Generating Mechanisms Across
487 the United States. *Geophys. Res. Letts.*, 43, 4382-4390, doi: 10.1002/2016GL068070, 2016.

488

489 Byrd, J. G.: Calamity: The Heppner Flood of 1903. University of Washington Press, 2014.

490

491 Chegwiddden, O. S., B. Nijssen, D.E. Rupp, and P.W. Mote, Hydrologic Response of the Columbia River System
492 to Climate Change [Data set]. Zenodo. doi:10.5281/zenodo.854763, 2017.

493

494 Chegwiddden, O. S., B. Nijssen, D.E. Rupp, J.R. Arnold, M.P. Clark, J.J. Hamman, S. Kao, et al: How Do Modeling
495 Decisions Affect the Spread Among Hydrologic Climate Change Projections? Exploring a Large Ensemble of
496 Simulations Across a Diversity of Hydroclimates. *Earth's Future*, 7, 623–637, doi: 10.1029/2018EF001047, 2019.

497

498 Chegwiddden, O.S., D.E. Rupp, B. Nijssen: Climate change alters flood magnitudes and mechanisms in climati-
499 cally-diverse headwaters across the northwestern United States. *Environmental Research Letters*, doi:
500 [10.1088/1748-9326/ab986f](https://doi.org/10.1088/1748-9326/ab986f), 2020.

501

502 Clark, M. P., Nijssen, B., Lundquist, J. D., Kavetski, D., Rupp, D. E., Woods, R. A., ... & Arnold, J. R. (2015). A
503 unified approach for process-based hydrologic modeling: 1. Modeling concept. *Water Resources Research*, 51(4),
504 2498-2514.

505

506 Do, H. X., F. Zhao, S. Westra, M. Leonard, L. Gudmundsson, J. Chang, P. Ciais, D. Gerten, S.N. Gosling, H.M.
507 Schmied, T. Stacke, B.J.E. Stanislas, and Y. Wada: Historical and Future Changes in Global Flood Magnitude –
508 Evidence from a Model-Observation Investigation. *Hydrol. Earth Syst. Sci. Discuss*, doi: 10.5194/hess-2019-388,
509 in review, 2019.

510
511
512
513
514
515
516
517
518
519
520
521
522
523
524
525
526
527
528
529
530
531
532
533
534
535
536
537
538

Douglas, E.M., R.M. Vogel, and C.N. Kroll: Trends in Floods and Low Flows in the United States: Impact of Spatial Correlation. *Journal of Hydrology*, doi: 10.1016/S0022-1694(00)00336-X, 2000.

Eyring, V., S. Bony, G.A. Meehl, C.A. Senior, B. Stevens, R.J. Stouffer, and K.E. Taylor: Overview of the Coupled Model Intercomparison Project Phase 6 (CMIP6) Experimental Design and Organization. *Geosci. Model Dev.*, 9, 1937-1958, doi: 10.5194/gmd-9-1937-2016, 2016.

Fritze, H., I.T. Stewart, and E. J. Pebesma: Shifts in Western North American Snowmelt Runoff Regimes for the Recent Warm Decades. *Journal of Hydrometeorology*, doi: 10.1175/2011JHM1360.1, 2011.

Gangrade, Sudershan & Kao, Shih-Chieh & McManamay, Ryan. (2020). Multi-model Hydroclimate Projections for the Alabama-Coosa-Tallapoosa River Basin in the Southeastern United States. *Scientific Reports*. 10.1038/s41598-020-59806-6.

Goode, J.R., J.M. Buffington, D. Tonina, D.J. Isaak, R.F. Thurow, S. Wenger, D. Nagel, C. Luce, D. Tetzlaff, and C. Soulsby: Potential effects of climate change on streambed scour and risks to salmonid survival in snow-dominated mountain basins. *Hydrological Processes*, 27, 750-765, doi: 10.1002/hyp.9728.

Gutmann, E., T. Pruitt, M. P. Clark, L. Brekke, J.R. Arnold, D. A. Raff, and R.M. Rasmussen: An Intercomparison of Statistical Downscaling Methods Used for Water Resource Assessments in the United States. *Water Resources Research*, 50, 7167–7186, doi: 10.1002/2014WR015559, 2014.

Hamlet, A.F., and D.P. Lettenmaier: Effects of 20th Century Warming and Climate Variability on Flood Risk in the Western U.S. *Water Resour. Res.*, 43, W06427, doi: 10.1029/2006WR005099, 2007.

Hamlet, A.F., P.W. Mote, M.P. Clark, and D.P. Lettenmaier, 2005: Effects of precipitation and temperature variability on snowpack trends in the western United States, *J. Climate*, 18, 4545–4561.

539 Hamlet, A.F., E.P. Salathé, and P. Carrasco: Statistical Downscaling Techniques for Global Climate Model Sim-
540 ulations of Temperature and Precipitation with Application to Water Resources Planning Studies. Chapter 4 in Fi-
541 nal Report for the Columbia Basin Climate Change Scenarios Project, Climate Impacts Group, Center for Science
542 in the Earth System, Joint Institute for the Study of the Atmosphere and Ocean, University of Washington, Seattle,
543 2010.
544

545 Hamman, J., and B. Nijssen: VIC 4.2.glacier. Retrieved from [https://github.com/UW-Hydro/VIC/tree/sup-](https://github.com/UW-Hydro/VIC/tree/support/VIC.4.2.glacier)
546 [port/VIC.4.2.glacier](https://github.com/UW-Hydro/VIC/tree/support/VIC.4.2.glacier), 2015.
547

548 Hawkins, E., and R. Sutton: The potential to narrow uncertainty in regional climate predictions. Bulletin of the
549 American Meteorological Society, 90, 1095–1108, doi: 10.1175/2009BAMS2607.1, 2009.
550

551 Huang, S., Kumar, R., Rakovec, O., Aich, V., Wang, X., Samaniego, L., ... & Krysanova, V. (2018). Multimodel
552 assessment of flood characteristics in four large river basins at global warming of 1.5, 2.0 and 3.0 K above the
553 pre-industrial level. Environmental Research Letters, 13(12), 124005.
554

555 Kundzewicz, Z.W., S. Kanae, S.I. Seneviratne, J. Handmer, N. Nicholls, P. Peduzzi, R. Mechler, L.M. Bouwer,
556 N. Arnell, K. Mach, R. Muir-Wood, G.R. Brakenridge, W. Kron, G. Benito, Y. Honda, K. Takahashi, and B.
557 Sherstyukov: Flood Risk and Climate Change: Global and Regional Perspectives. Hydrological Sciences Journal,
558 59, 1-28, doi: 10.1080/02626667.2013.857411, 2014.
559

560 Lute, A. C., J.T. Abatzoglou, and K.C. Hegewisch: Projected Changes in Snowfall Extremes and Interannual Var-
561 iability of Snowfall in the Western United States. Water Resources Research, 51, 960–972, doi:
562 10.1002/2014WR016267, 2015.
563

564 Mearns, L.O., Sain, S., Leung, L.R. et al. Climate change projections of the North American Regional Climate
565 Change Assessment Program (NARCCAP). Climatic Change 120, 965–975 (2013).
566 <https://doi.org/10.1007/s10584-013-0831-3>.
567

568 Musselman, K., Clark, M., Liu, C. et al. Slower snowmelt in a warmer world. *Nature Clim Change* 7, 214–219
569 (2017). <https://doi.org/10.1038/nclimate3225>
570

571 Najafi, M.R., and H. Moradkhani: Multi-model Ensemble Analysis of Runoff Extremes for Climate Change Im-
572 pact Assessments. *Journal of Hydrology*, 525, 352-361, doi: 10.1016/j.jhydrol.2015.03.045, 2015.
573

574 Parker, L. E., & Abatzoglou, J. T. (2016). Spatial coherence of extreme precipitation events in the Northwestern
575 United States. *International Journal of Climatology*, 36(6), 2451-2460.
576

577 River Management Joint Operating Committee: Climate and Hydrology Datasets for RMJOC Long-term Planning
578 Studies. Second edition: Part 1—Hydroclimate Projections and Analyses, retrieved from
579 <https://www.bpa.gov/p/Generation/Hydro/Pages/Climate-Change-FCRPS-Hydro.aspx>, 2018.
580

581 Rupp, D. E., J.T. Abatzoglou, K.C. Hegewisch, and P.W. Mote: Evaluation of CMIP5 20th Century Climate
582 Simulations for the Pacific Northwest USA. *Journal of Geophysical Research: Atmospheres*, 118, 10,884–10,906,
583 doi: 10.1002/jgrd.50843, 2013.
584

585 Rupp, D.E., J.T. Abatzoglou, and P.W Mote: Projections of 21st Century Climate of the Columbia River Basin.
586 *Clim. Dyn.*, doi: 10.1007/s00382-016-3418-7, 2016.
587

588 Salathé, E. P., et al: Estimates of Twenty-First-Century Flood Risk in the Pacific Northwest Based on Regional
589 Climate Model Simulations. *J. Hydrometeor*, 15, 1881–1899, 2014.
590

591 Serinaldi, F., and C.G. Kilsby: Stationarity is Undead: Uncertainty Dominates the Distribution of Extremes. *Ad-
592 vances in Water Resources*, doi: 10.1016/j.advwatres.2014.12.013, 2015.
593

594 Sharma, A., C. Wasko, and D.P. Lettenmaier: If Precipitation Extremes Are Increasing, Why Aren't Floods? *Wa-
595 ter Resources Research*, doi: 10.1029/2018WR023749, 2018.
596

597 Stewart, I. T., D.R. Cayan, and M.D. Dettinger: Changes Toward Earlier Streamflow Timing Across Western
598 North America. *J. Climate*, 18, 1136–1155, 2005.
599

600 Surfleet, C. G., and D. Tullos, D.: Variability in Effect of Climate Change on Rain-on-Snow Peak Flow Events
601 in a Temperate Climate. *Journal of Hydrology*, 479, 24-34, doi: 10.1016/j.jhydrol.2012.11.021, 2013.
602

603 Thober, S., Kumar, R., Wanders, N., Marx, A., Pan, M., Rakovec, O., Samaniego, L., Sheffield, J., Wood, E.F.
604 and Zink, M., 2018. Multi-model ensemble projections of European river floods and high flows at 1.5, 2, and 3
605 degrees global warming. *Environmental Research Letters*, 13(1), p.014003.
606

607 Tohver, I., A. F. Hamlet, and S.-Y. Lee: Impacts of 21st Century Climate Change on Hydrologic Extremes in the
608 Pacific Northwest Region of North America. *J. Amer. Water Resour. Assoc.*, doi: 10.1111/jawr.12199, 2014.
609

610 Vano, J. A., J. B. Kim, D. E. Rupp, and P. W. Mote: Selecting Climate Change Scenarios Using Impact-relevant
611 Sensitivities. *Geophys. Res. Lett.*, 42, 5516–5525, doi: 10.1002/2015GL063208, 2015.
612

613 Vormoor, K., Lawrence, D., Heistermann, M., & Bronstert, A. (2015). Climate change impacts on the seasonality
614 and generation processes of floods--projections and uncertainties for catchments with mixed snowmelt/rainfall
615 regimes. *Hydrology & Earth System Sciences*, 19(2).
616

617 Wood, A., L. Leung, V. Sridhar, and D. Lettenmaier: Hydrologic Implications of Dynamical and Statistical Ap-
618 proaches to Downscaling Climate Model Outputs. *Clim. Change*, 62, 189–216, 2004.
619

620 **Figure captions.**

621

622 **Figure 1.** Domain of hydrologic simulations used in this paper, with colors indicating elevation of each grid cell,
623 major rivers highlighted in blue, and numbers indicating locations of streamflow points highlighted in Figures 6-
624 11, and Table 1. See Chegwiddden et al. (2017, 2019) for all streamflow locations plotted in Figure 5.

625 **Figure 2.** Generalized Extreme Value fit of annual maximum daily streamflow from 50 years of simulation using
626 output from one GCM (HadGEM2-ES), one hydrologic model (PRMS), for the Willamette River at Portland. Red
627 and blue dots/ lines indicate the annual values and GEV fit for the 1950-99 ‘past’ and 2050-99 ‘future’ periods.
628

629 **Figure 3.** Comparison of 10-year (a, b, c) and 100-year (d, e, f) flood magnitudes from the observationally derived
630 NRNI and the 40 climate-hydrologic model simulations, for 1950-2008, for select locations on the rivers as shown.
631

632 **Figure 4.** Statistical representations of the variation through the water year of the timing of flood events, 1950-
633 2008, for NRNI (blue) and the 40 simulations of 1950-2008 with the climate-hydrology modeling system (green).
634 To create each curve, the dates of the 5 highest streamflows in the period of record are tallied, and the resulting
635 distributions smoothed. Long dashed lines indicate median date, short dashed lines the lowest and highest quarti-
636 les. MCD= Mica Dam (upper Columbia), TDA= The Dalles (lower Columbia, between the confluences of the
637 Snake and Willamette), LGS = Little Goose (lower Snake), BRN=Brownlee, SVN=T. W. Sullivan (lower
638 Willamette near Portland), DEX=Dexter (middle fork Willamette).
639

640 **Figure 5.** Discharge ratios (future:past) versus centroid of timing (day on which 50% of water-year streamflow
641 has passed, an indicator of snow dominance) for all 396 locations and four return periods. For each location, the
642 average of 40 ensemble member ratios calculated from GEV distribution fitting from 50-year windows for the
643 future (2050-2099) and past (1950-1999) time periods is shown. Points are sized by average daily streamflow and
644 colored by the coefficient of variation of the 40 ratios.
645

646 **Figure 6.** As in Figure 5 but only for points on the indicated rivers. Dashed lines indicate tributaries: 9-12 are on
647 the Middle Fork Willamette, 15-17 on the McKenzie; tributaries of the Snake are the Grand Ronde (14), Clear-
648 water (17) and Salmon (24). In the lower panel, the Grand Ronde and Salmon are clearly distinguished by a black

649 circle around their perimeter. Table 1 translates the codes in the legend into named locations and shows the nu-
650 merical values represented in the figure. As is evident from both snow-dominance and size, locations are ordered
651 downstream to upstream from left to right for each river.

652

653 **Figure 7.** Averaged (large circles) and individual ensemble member (small colored circles) discharge ratios for
654 simulated streamflow locations along the mainstem Columbia River for the 10-year (top) and 100-year (bottom)
655 return periods. As shown in the legend, the color of the dots distinguishes results by hydrologic model setup.

656

657 **Figure 8.** Average ratios of all 40 ensemble members (large circles) and the average of 4 hydrologic model re-
658 sults for each GCM (symbols), shown for simulated streamflow locations along the Willamette (top), Snake
659 (middle), and the mainstem Columbia (bottom) for 100-year return periods. GCMs are ordered in the legend
660 by their ranking in Rupp et al. (2017), representing their ability to simulate Northwest climate.

661

662 **Figure 9.** As in Figure 8 but averaged by hydrologic model, for 10-year return period, and combined into one
663 panel.

664

665 **Figure 10.** ANOVA results for select locations on the indicated rivers, for climate and hydrologic factors (and
666 the residual). Charts are numbered to correspond with their location in Figure 6, with the most-downstream loca-
667 tion at the top.

668

669 **Figure 11.** Statistical representations of the variation through the water year of the timing of flood events. For
670 each of the 40 simulations, the dates of the 5 highest streamflows in the 50-year past (blue) and future (green)
671 windows are tallied, and the resulting distributions smoothed. Long dashed lines indicate median date, short
672 dashed lines the lowest and highest quartiles.

673

674

675

676

677

Table 1 Information about locations featured in this paper - location, river, and discharge ratios

River	UW Key	Description	10-year flood discharge ratios				100-year flood discharge ratios			
			Avg.	Coeff. of Var.	Min	Max	Avg.	Coeff. of Var.	Min	Max
Chehalis	CHEGR	Chehalis R nr Grand Mound	1.21	0.09	1.03	1.42	1.34	0.18	0.87	2.07
Chehalis	CHE	Chehalis R at Porter	1.21	0.08	1.03	1.40	1.31	0.16	0.91	1.89
Willamette	SVN	T.W. Sullivan	1.33	0.09	1.07	1.64	1.39	0.22	0.87	2.39
Willamette	WILPO	Portland	1.34	0.09	1.08	1.69	1.40	0.23	0.86	2.47
Willamette	WILLA	Newberg	1.34	0.09	1.09	1.66	1.40	0.22	0.88	2.44
Willamette	SLM	Salem	1.37	0.09	1.10	1.70	1.43	0.22	0.84	2.52
Willamette	ALBO	Albany	1.40	0.09	1.11	1.73	1.47	0.20	0.89	2.40
Willamette	HARO	Harrisburg	1.45	0.10	1.18	1.86	1.50	0.22	0.88	2.37
Willamette	JASO	Middle fork @ Jasper	1.50	0.14	1.20	2.13	1.57	0.23	0.93	2.68
Willamette	DEX	Dexter	1.55	0.16	1.17	2.33	1.61	0.22	1.05	2.67
Willamette	HCR	Hills Creek	1.57	0.18	1.15	2.46	1.60	0.25	1.10	3.18

River	UW Key	Description	10-year flood discharge ratios				100-year flood discharge ratios			
			Avg.	Coeff. of Var.	Min	Max	Avg.	Coeff. of Var.	Min	Max
Willamette	WILNF	Oakridge	1.57	0.18	1.16	2.45	1.63	0.24	1.09	2.88
Willamette	EUGO	WR at Eugene (NWP)	1.50	0.12	1.26	2.04	1.54	0.22	0.88	2.57
Willamette	WAV	Walterville	1.54	0.13	1.29	2.13	1.55	0.18	1.04	2.23
Willamette	LEA	Leaburg	1.56	0.14	1.28	2.23	1.56	0.18	1.05	2.34
Willamette	VIDO	McKenzie nr Vida	1.57	0.15	1.28	2.32	1.58	0.19	1.02	2.41
Willamette	COT	Cottage Grove	1.25	0.11	0.97	1.69	1.39	0.29	0.78	2.38
Snake	IHR	Ice Harbor	1.20	0.13	0.92	1.75	1.26	0.28	0.79	2.84
Snake	LMN	Lower Monumental	1.20	0.13	0.92	1.76	1.26	0.28	0.78	2.77
Snake	LGS	Little Goose	1.19	0.13	0.92	1.77	1.26	0.28	0.78	2.83
Snake	LWG	Lower Granite	1.19	0.13	0.92	1.77	1.25	0.29	0.78	2.89
Snake	ANA	Anatone	1.24	0.14	0.95	1.74	1.29	0.29	0.78	2.84
Snake	LIM	Lime Point	1.23	0.14	0.94	1.73	1.28	0.30	0.76	2.81

River	UW Key	Description	10-year flood discharge ratios				100-year flood discharge ratios			
			Avg.	Coeff. of Var.	Min	Max	Avg.	Coeff. of Var.	Min	Max
Snake	HCD	Hells Canyon	1.40	0.18	1.01	2.11	1.55	0.38	0.87	3.62
Snake	OXB	Oxbow	1.41	0.18	1.01	2.11	1.56	0.38	0.86	3.65
Snake	BRN	Brownlee Dam	1.41	0.18	1.01	2.12	1.56	0.37	0.86	3.63
Snake	WEII	Weiser, ID	1.39	0.18	1.02	2.09	1.53	0.35	0.86	3.28
Snake	SNYI	Nyssa, OR	1.40	0.18	1.04	2.16	1.52	0.33	0.89	3.21
Snake	SWAI	Murphy, ID	1.37	0.19	0.98	2.09	1.48	0.33	0.84	3.24
Snake	CJSTR	CJ Strike Dam	1.37	0.19	0.97	2.08	1.48	0.32	0.86	3.08
Snake	SKHI	King Hill, ID	1.37	0.19	0.96	2.08	1.48	0.32	0.85	2.84
Snake	SNKBL WLSAL MON	Hagerman, ID	1.35	0.18	0.93	2.05	1.46	0.31	0.83	2.66
Snake	BUHL	Buhl, ID	1.35	0.19	0.91	2.05	1.46	0.32	0.73	2.54
Snake	KIMI	Kimberly, ID	1.33	0.19	0.89	2.03	1.44	0.33	0.74	2.47
Snake	MILI	Milner, ID	1.33	0.19	0.88	2.04	1.44	0.34	0.73	2.52

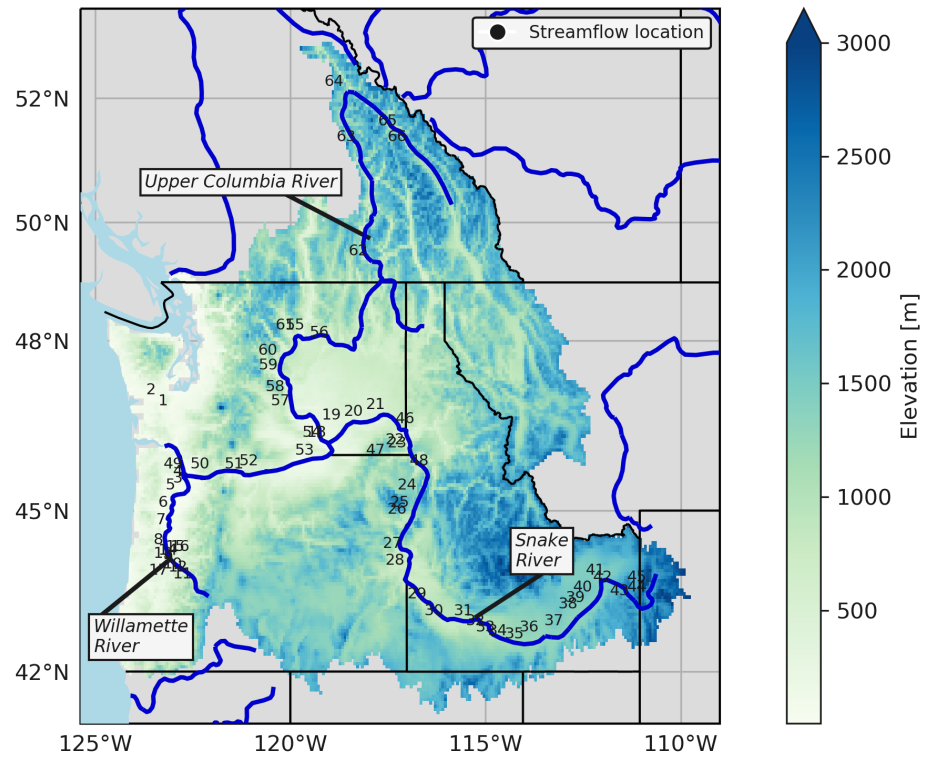
River	UW Key	Description	10-year flood discharge ratios				100-year flood discharge ratios			
			Avg.	Coeff. of Var.	Min	Max	Avg.	Coeff. of Var.	Min	Max
Snake	MINI	Minidoka, ID	1.33	0.19	0.86	2.02	1.45	0.33	0.70	2.53
Snake	AMFI	Neeley American Falls	1.32	0.19	0.85	1.99	1.45	0.34	0.67	2.69
Snake	BFTI	nr Blackfoot, ID	1.31	0.19	0.84	1.96	1.43	0.34	0.67	2.72
Snake	SNAI	nr Blackfoot, ID	1.30	0.19	0.84	1.95	1.43	0.34	0.67	2.69
Snake	SHYI	Shelley, ID	1.29	0.18	0.84	1.92	1.40	0.33	0.69	2.62
Snake	LORI	Lorenzo, ID	1.28	0.19	0.86	1.91	1.38	0.34	0.69	2.52
Snake	HEII	Heise, ID	1.28	0.18	0.86	1.91	1.37	0.33	0.70	2.53
Snake	PALI	Irwin Palisades	1.28	0.19	0.87	1.95	1.37	0.34	0.71	2.60
Snake	JKSY	Jackson, WY	1.26	0.15	0.89	1.73	1.35	0.30	0.80	2.46
Snake	SRMO	Moose, WY	1.25	0.13	0.91	1.59	1.35	0.25	0.83	2.34
Grand Ronde	TRY	Troy	1.48	0.19	1.09	2.55	1.68	0.34	1.01	4.38
Salmon	WHB	White Bird	1.07	0.13	0.83	1.57	1.09	0.33	0.72	2.81

River	UW Key	Description	10-year flood discharge ratios				100-year flood discharge ratios			
			Avg.	Coeff. of Var.	Min	Max	Avg.	Coeff. of Var.	Min	Max
Columbia	CRVAN	Vancouver	1.03	0.09	0.90	1.22	1.05	0.13	0.80	1.49
Columbia	BON	Bonneville	1.03	0.09	0.90	1.21	1.05	0.13	0.80	1.49
Columbia	TDA	The Dalles	1.03	0.08	0.90	1.20	1.05	0.13	0.81	1.52
Columbia	JDA	John Day	1.02	0.08	0.90	1.19	1.05	0.13	0.80	1.51
Columbia	MCN	McNary Dam	1.02	0.08	0.89	1.18	1.05	0.13	0.80	1.45
Columbia	CLKEN	Clover Island @ Kennewick	1.03	0.10	0.82	1.22	1.11	0.14	0.84	1.49
Columbia	CHJ	Chief Joseph	1.06	0.11	0.83	1.25	1.15	0.15	0.85	1.70
Columbia	GCL	Grand Coulee	1.06	0.11	0.83	1.25	1.14	0.14	0.84	1.66
Columbia	PRD	Priest Rapids	1.04	0.10	0.82	1.22	1.11	0.13	0.84	1.54
Columbia	WAN	Wanapum	1.04	0.10	0.82	1.22	1.11	0.14	0.84	1.58
Columbia	RIS	Rock Island	1.04	0.10	0.82	1.23	1.12	0.14	0.84	1.60
Columbia	RRH	Rocky Reach	1.05	0.10	0.83	1.23	1.13	0.14	0.84	1.61

River	UW Key	Description	10-year flood discharge ratios				100-year flood discharge ratios			
			Avg.	Coeff. of Var.	Min	Max	Avg.	Coeff. of Var.	Min	Max
Columbia	WEL	Wells Dam	1.05	0.10	0.83	1.24	1.14	0.14	0.85	1.63
Columbia	ARD	Hugh Keenleyside (Arrow)	1.13	0.12	0.87	1.43	1.24	0.21	0.69	1.83
Columbia	RVC	Revelstoke	1.19	0.12	0.91	1.62	1.36	0.23	0.69	2.08
Columbia	MCD	Mica Dam	1.22	0.12	0.94	1.66	1.41	0.24	0.72	2.12
Columbia	DONAL	Donald	1.28	0.14	1.02	1.79	1.55	0.25	0.94	2.38
Columbia	CRNIC	Nicholson	1.25	0.13	0.98	1.61	1.47	0.23	0.94	2.39
Clearwater	SPD	Spalding, ID	1.15	0.15	0.85	1.78	1.32	0.30	0.80	2.63
Clearwater	DWR	Dworshak Dam, ID	1.14	0.12	0.86	1.55	1.30	0.24	0.89	2.22
Santiam	JFFO	Santiam R nr Jefferson	1.40	0.10	1.14	1.81	1.41	0.25	0.81	2.27
Kootenay	COR	Corra Linn Dam, BC	1.08	0.12	0.85	1.31	1.15	0.16	0.79	1.67
Kootenai	LIB	Libby Dam, MT	1.17	0.14	0.92	1.52	1.32	0.22	0.85	2.01
Kootenay	BFE	Bonner's Ferry, ID	1.13	0.13	0.89	1.45	1.26	0.20	0.83	2.02

River	UW Key	Description	10-year flood discharge ratios				100-year flood discharge ratios			
			Avg.	Coeff. of Var.	Min	Max	Avg.	Coeff. of Var.	Min	Max
Pend Oreille	ALF	Albeni Falls, ID	1.26	0.14	0.96	1.68	1.65	0.30	1.02	2.97
Flathead	CFM	Columbia Falls, MT	1.24	0.13	0.94	1.63	1.65	0.26	1.01	3.19
Flathead	HGH	Hungry Horse Dam, MT	1.30	0.13	1.04	1.70	1.78	0.29	1.16	3.56
Yakima	KIOW	Yakima, WA	1.82	0.21	1.35	3.11	2.28	0.30	1.57	4.39

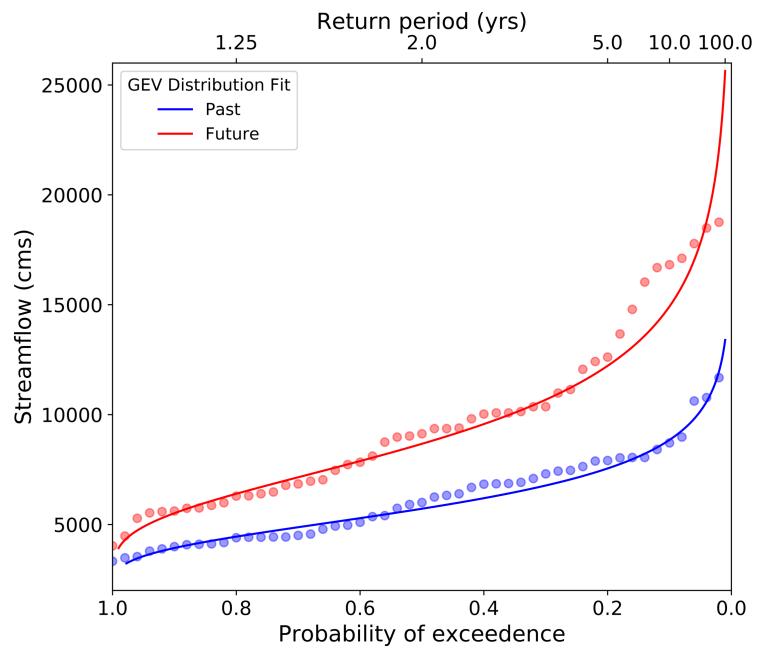
678
679



565

566

567 **Figure 1.** Domain of hydrologic simulations used in this paper, with colors indicating elevation of each grid cell,
 568 major rivers highlighted in blue, and numbers indicating locations of streamflow points highlighted in Figures 4-
 569 9, and Table 1. See Chegwiddden et al. (2017, 2019) for all streamflow locations plotted in Figure 3. Digital ele-
 570 vation data are in the public domain, obtained from <https://www2.usgs.gov/science/cite-view.php?cite=1530>



571

572 **Figure 2.** Generalized Extreme Value fit of annual maximum daily flow from 50 years of simulation using output
 573 from one GCM (HadGEM2-ES), one hydrologic model (PRMS), for the Willamette River at Portland. Red and
 574 blue dots/ lines indicate the annual values and GEV fit for the 1950-99 ‘past’ and 2050-99 ‘future’ periods.

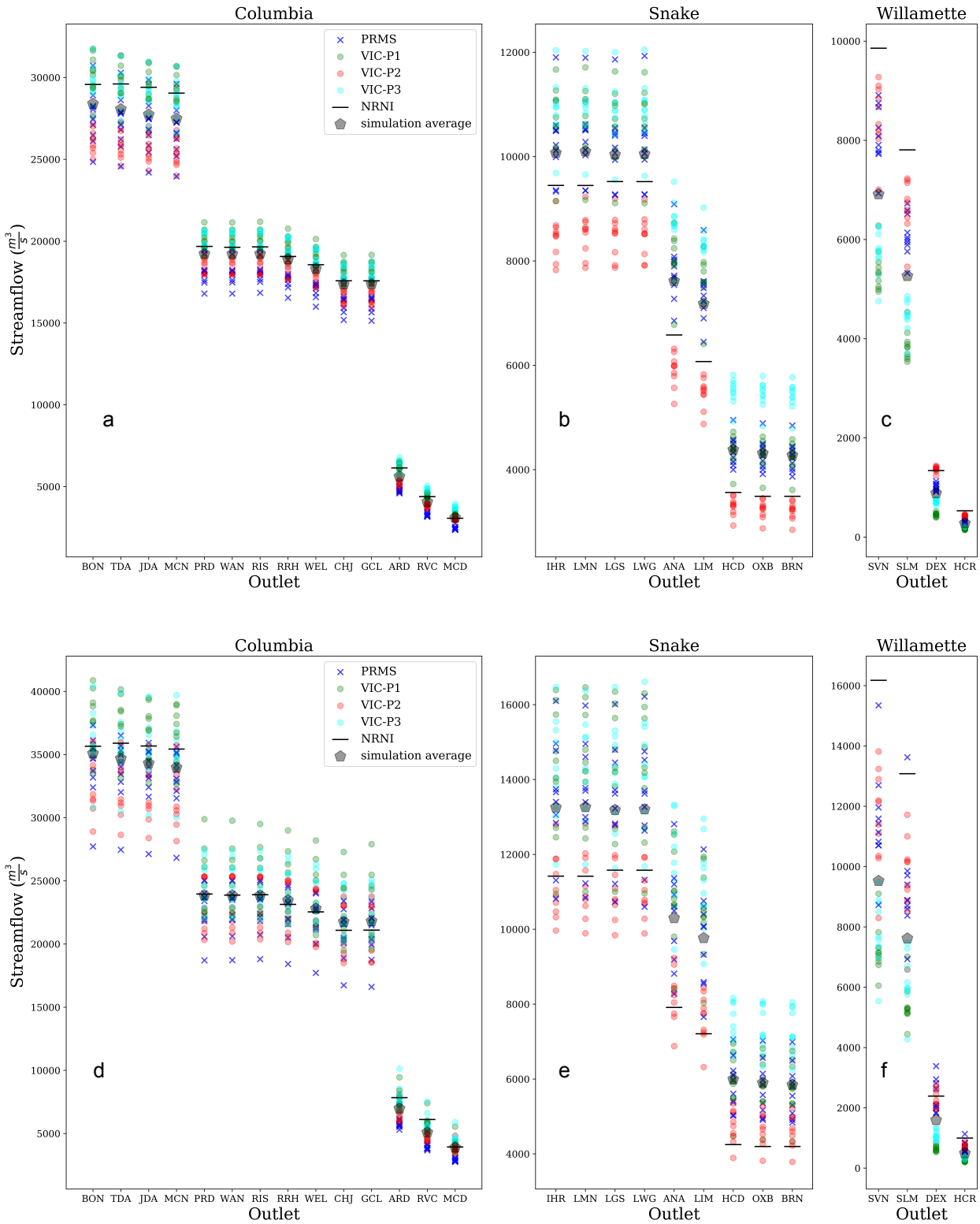


Figure 3. Comparison of 10-year (a, b, c) and 100-year (d, e, f) flood magnitudes from the observationally derived NRNI and the 40 climate-hydrologic model simulations, for 1950-2008, for select locations on the rivers as shown.

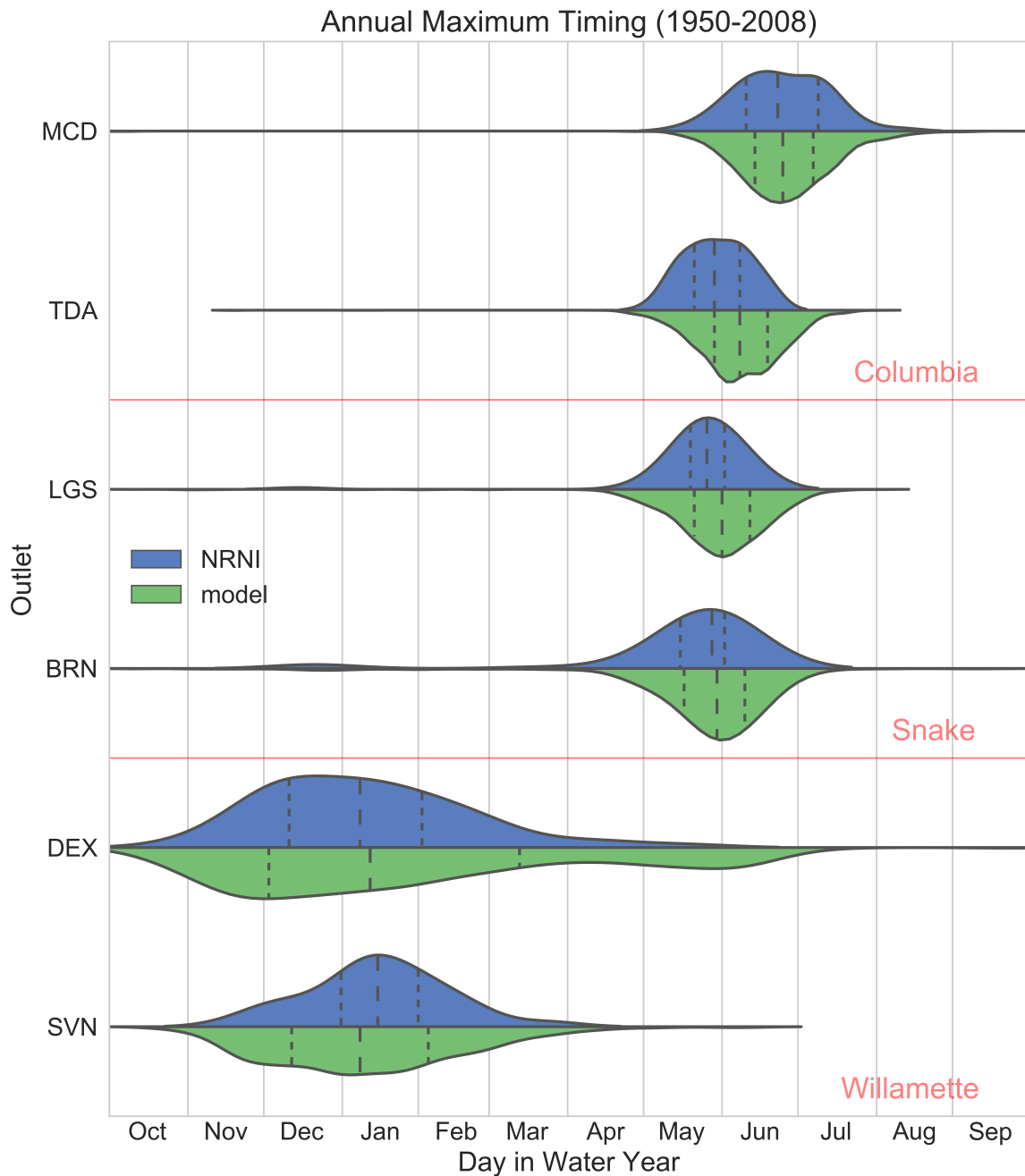
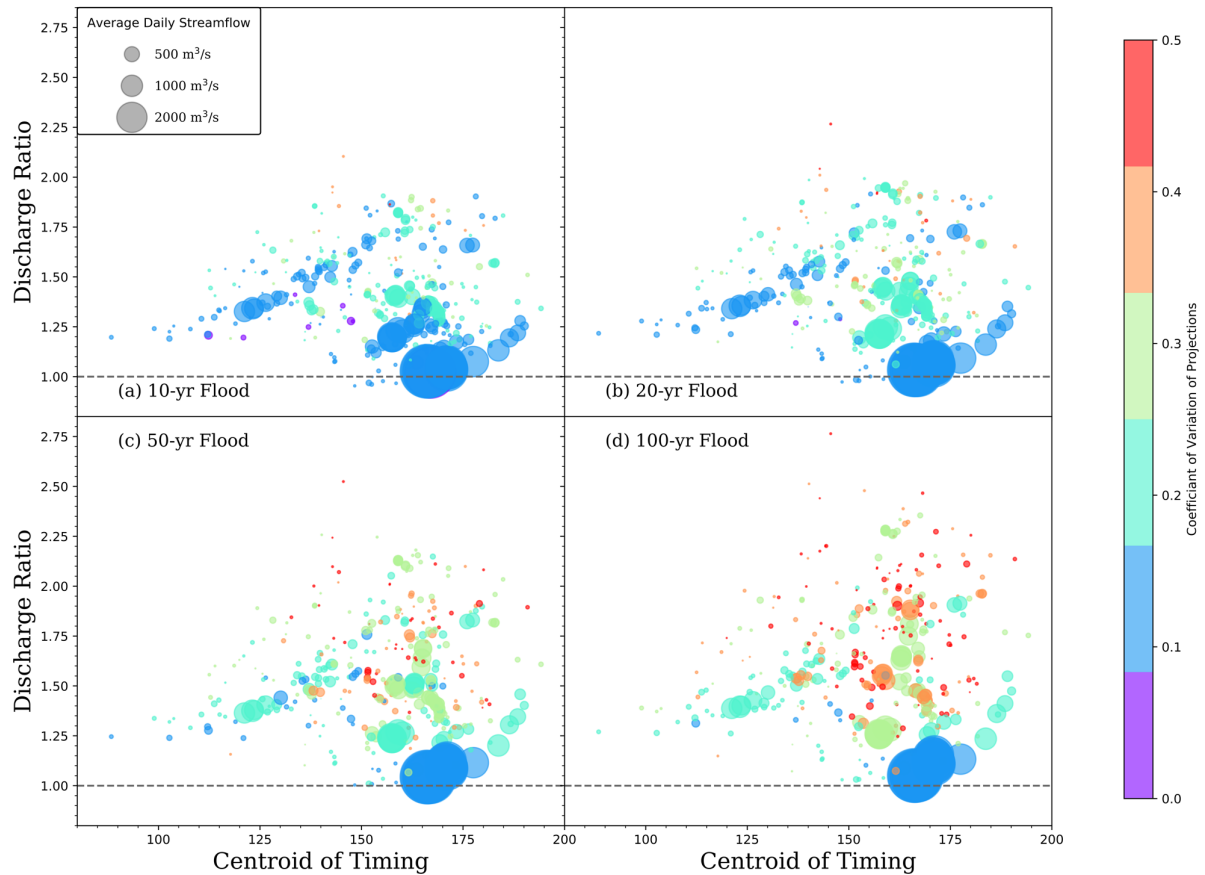


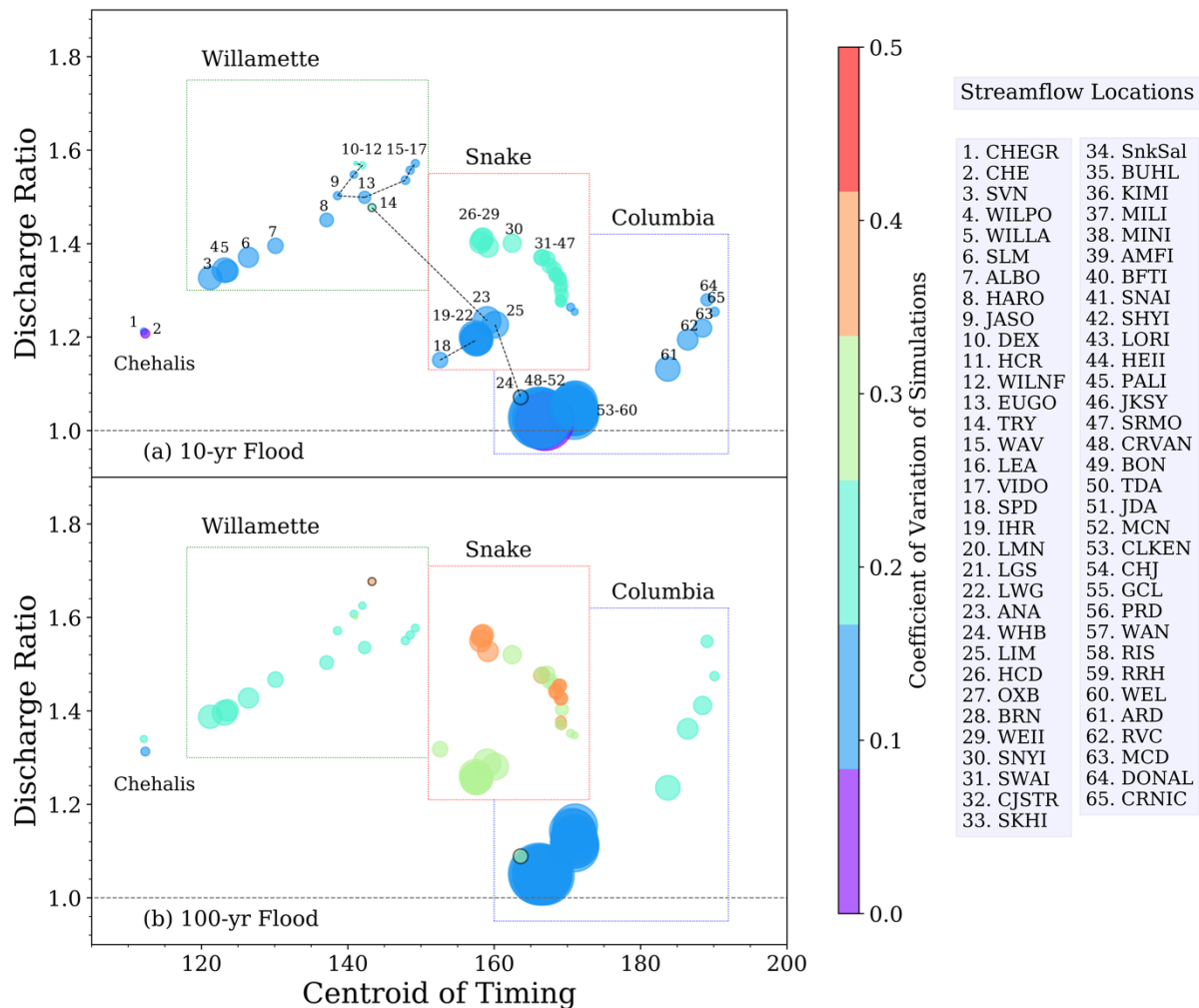
Figure 4. Statistical representations of the variation through the water year of the timing of flood events, 1950-2008, for NRNI (blue) and the 40 simulations of 1950-2008 with the climate-hydrology modeling system (green). To create each curve, the dates of the 5 highest streamflows in the period of record are tallied, and the resulting distributions smoothed. Long dashed lines indicate median date, short dashed lines the lowest and highest quartiles. MCD= Mica Dam (upper Columbia), TDA= The Dalles (lower Columbia, between the confluences of the Snake and Willamette), LGS = Little Goose (lower Snake), BRN=Brownlee, SVN=T. W. Sullivan (lower Willamette near Portland), DEX=Dexter (middle fork Willamette).



575

576

577 **Figure 5.** Discharge ratios (future:past) versus centroid of timing (day on which 50% of water-year flow has
 578 passed, an indicator of snow dominance) for all 396 locations and four return periods. For each location, the
 579 average of 40 ensemble member ratios calculated from GEV distribution fitting from 50-year windows for the
 580 future (2050-2099) and past (1950-1999) time periods is shown. Points are sized by average daily streamflow and
 581 colored by the coefficient of variation of the 40 ratios.



583

584

585

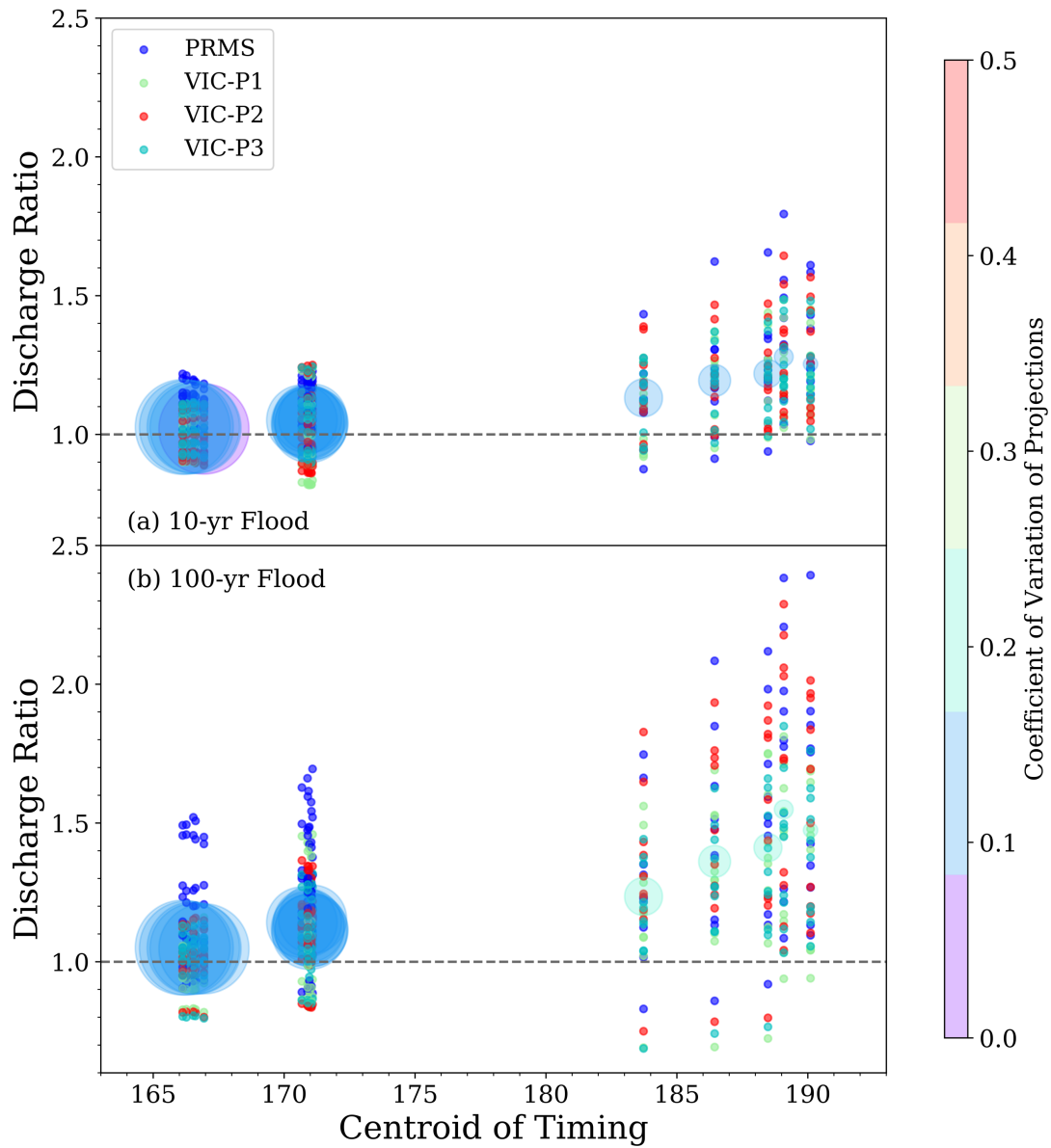
586

587

588

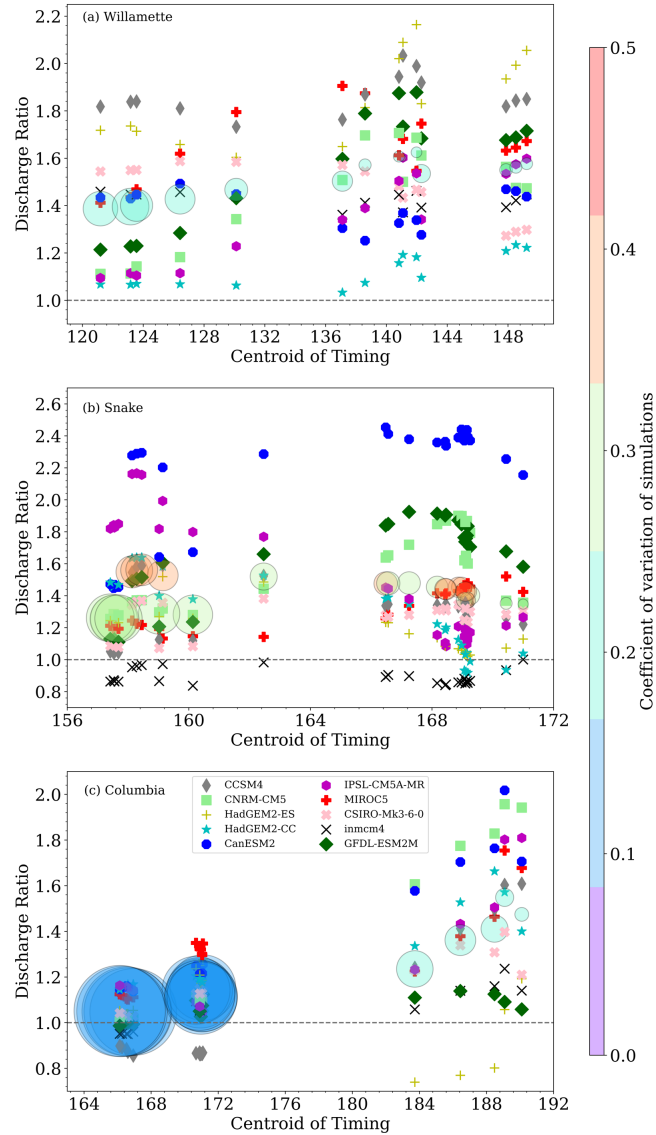
589

Figure 6. As in Figure 5 but only for points on the indicated rivers. Dashed lines indicate tributaries: 9-12 are on the Middle Fork Willamette, 15-17 on the McKenzie; tributaries of the Snake are the Grand Ronde (14), Clearwater (17) and Salmon (24). In the lower panel, the Grand Ronde and Salmon are clearly distinguished by a black circle around their perimeter. Table 1 translates the codes in the legend into named locations and shows the numerical values represented in the figure. As is evident from both snow-dominance and size, locations are ordered downstream to upstream from left to right for each river.

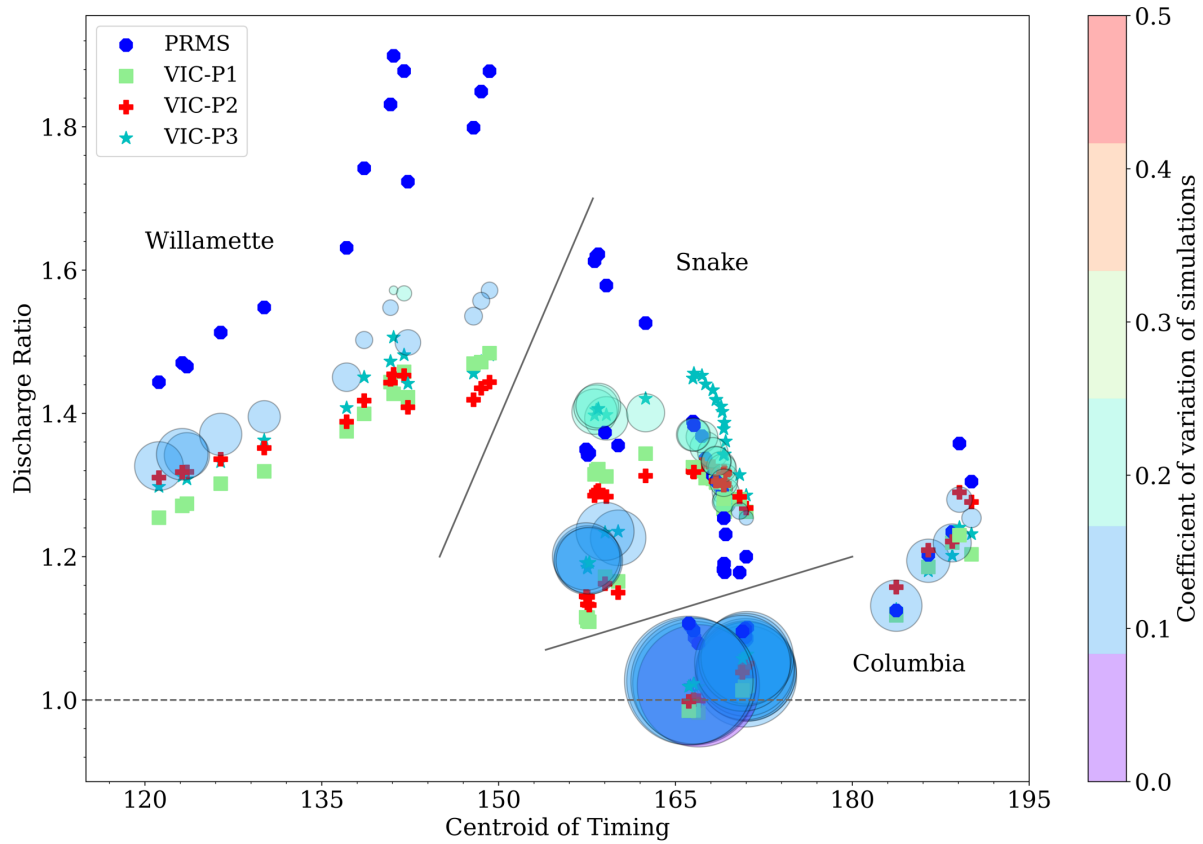


590

591 **Figure 7.** Averaged (large circles) and individual ensemble member (small colored circles) discharge ratios for
 592 simulated streamflow locations along the mainstem Columbia River for the 10-year (top) and 100-year (bottom)
 593 return periods. As shown in the legend, the color of the dots distinguishes results by hydrologic model setup.



594 **Figure 8.** Average ratios of all 40 ensemble members (large circles) and the average of 4 hydrologic model re-
 595 sults for each GCM (symbols), shown for simulated streamflow locations along the Willamette (top), Snake
 596 (middle), and the mainstem Columbia (bottom) for 100-year return periods. GCMs are ordered in the legend
 597 by their ranking in Rupp et al. (2017), representing their ability to simulate Northwest climate.

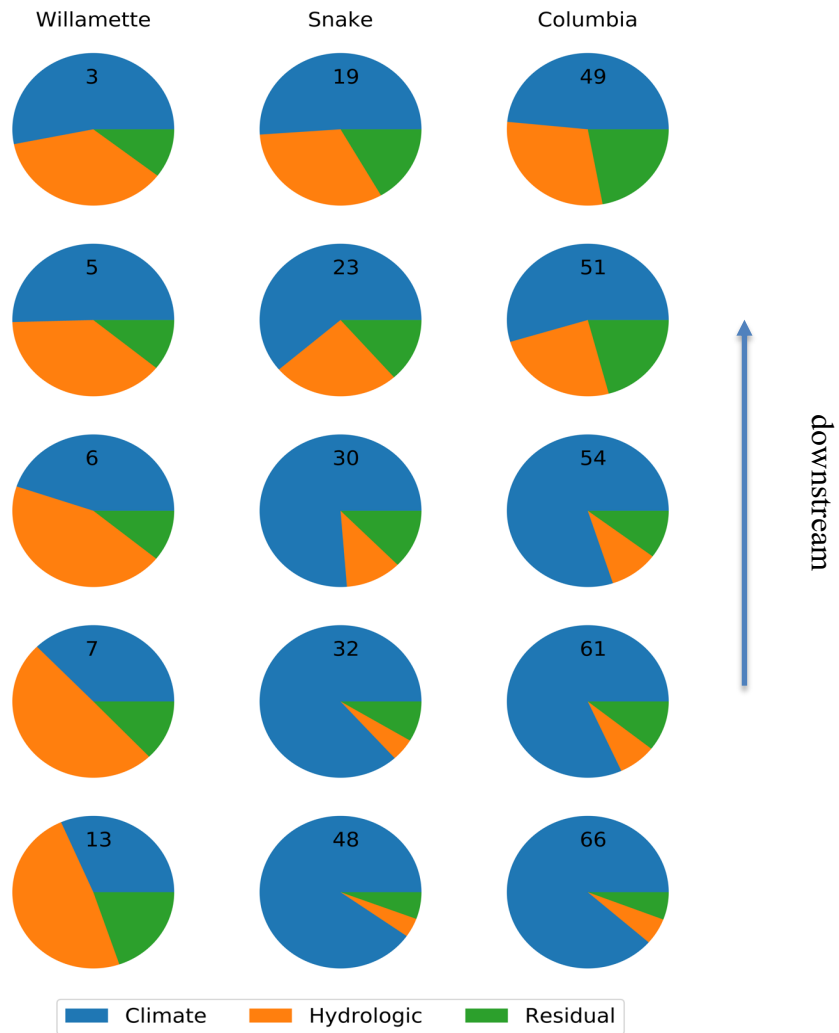


598

599

600

601 **Figure 9:** as in Figure 8 but averaged by hydrologic model, for 10-year return period, and combined into one
 602 panel.



603 **Figure 10.** ANOVA results for select locations on the indicated rivers, for climate and hydrologic factors (and the
 604 residual). Charts are numbered to correspond with their location in Figure 4, with the most-downstream location
 605 at the top. The Snake enters the Columbia after location #54.

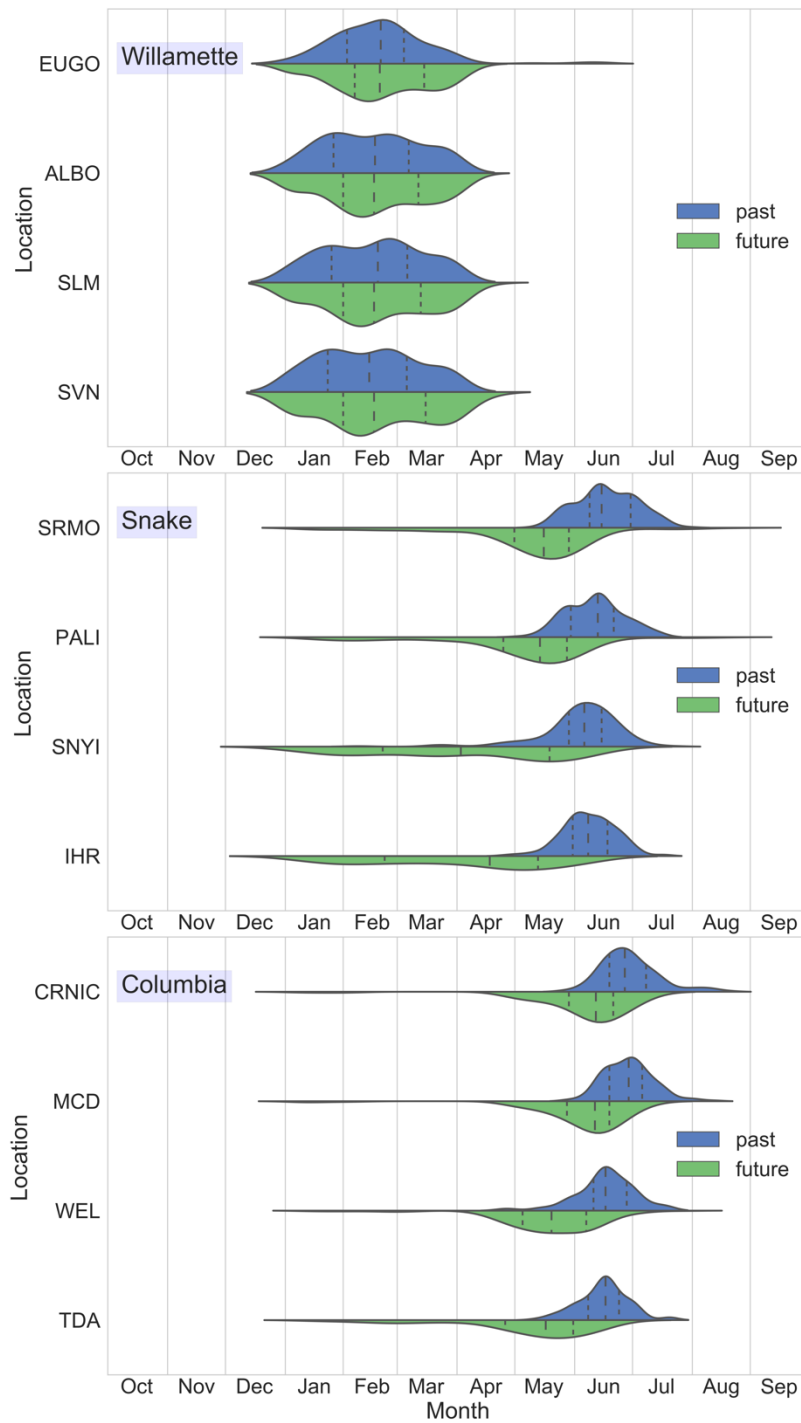


Figure 11. Statistical representations of the variation through the water year of the timing of flood events. For each of the 40 simulations, the dates of the 5 highest flows in the 50-year past (blue) and future (green) windows are tallied, and the resulting distributions smoothed. Long dashed lines indicate median date, short dashed lines the lowest and highest quartiles.